

Two waves of transcriptomic changes in periovulatory human granulosa cells

L.C. Poulsen^{1,*}, J.A. Bøtkjær², O. Østrup³, K.B. Petersen¹,
C. Yding Andersen², M.L. Grøndahl⁴, and A.L.M. Englund¹

¹Fertility Clinic, Zealand University Hospital, Lykkebækvej 14, 4600 Køge, Denmark, ²Laboratory of Reproductive Biology, University Hospital of Copenhagen, Rigshospitalet, Blegdamsvej 9, 2100 Copenhagen Ø, Denmark, ³Center for Genomic Medicine, Rigshospitalet, Blegdamsvej 9, 2100 Copenhagen Ø, Denmark, ⁴Fertility Clinic, University Hospital of Copenhagen, Herlev and Gentofte Hospital, Herlev Ringvej 75, 2730 Herlev, Denmark

*Correspondence address. E-mail: livlacour@hotmail.com

Submitted on August 27, 2019; resubmitted on February 5, 2020; editorial decision on February 17, 2020

STUDY QUESTION: How does the human granulosa cell (GC) transcriptome change during ovulation?

SUMMARY ANSWER: Two transcriptional peaks were observed at 12 h and at 36 h after induction of ovulation, both dominated by genes and pathways known from the inflammatory system.

WHAT IS KNOWN ALREADY: The crosstalk between GCs and the oocyte, which is essential for ovulation and oocyte maturation, can be assessed through transcriptomic profiling of GCs. Detailed transcriptional changes during ovulation have not previously been assessed in humans.

STUDY DESIGN, SIZE, DURATION: This prospective cohort study comprised 50 women undergoing fertility treatment in a standard antagonist protocol at a university hospital-affiliated fertility clinic in 2016–2018.

PARTICIPANTS/MATERIALS, SETTING, METHODS: From each woman, one sample of GCs was collected by transvaginal ultrasound-guided follicle aspiration either before or 12 h, 17 h or 32 h after ovulation induction (OI). A second sample was collected at oocyte retrieval, 36 h after OI. Total RNA was isolated from GCs and analyzed by microarray. Gene expression differences between the five time points were assessed by ANOVA with a random factor accounting for the pairing of samples, and seven clusters of protein-coding genes representing distinct expression profiles were identified. These were used as input for subsequent bioinformatic analyses to identify enriched pathways and suggest upstream regulators. Subsets of genes were assessed to explore specific ovulatory functions.

MAIN RESULTS AND THE ROLE OF CHANCE: We identified 13 345 differentially expressed transcripts across the five time points (false discovery rate, <0.01) of which 58% were protein-coding genes. Two clusters of mainly downregulated genes represented cell cycle pathways and DNA repair. Upregulated genes showed one peak at 12 h that resembled the initiation of an inflammatory response, and one peak at 36 h that resembled the effector functions of inflammation such as vasodilation, angiogenesis, coagulation, chemotaxis and tissue remodelling. Genes involved in cell–matrix interactions as a part of cytoskeletal rearrangement and cell motility were also upregulated at 36 h. Predicted activated upstream regulators of ovulation included FSH, LH, transforming growth factor β 1, tumour necrosis factor, nuclear factor kappa-light-chain-enhancer of activated B cells, coagulation factor 2, fibroblast growth factor 2, interleukin 1 and cortisol, among others. The results confirmed early regulation of several previously described factors in a cascade inducing meiotic resumption and suggested new factors involved in cumulus expansion and follicle rupture through co-regulation with previously described factors.

LARGE SCALE DATA: The microarray data were deposited to the Gene Expression Omnibus (www.ncbi.nlm.nih.gov/gds/, accession number: GSE133868).

LIMITATIONS, REASONS FOR CAUTION: The study included women undergoing ovarian stimulation and the findings may therefore differ from a natural cycle. However, the results confirm significant regulation of many well-established ovulatory genes from a series of previous studies such as amphiregulin, epiregulin, tumour necrosis factor α induced protein 6, tissue inhibitor of metalloproteinases 1 and plasminogen activator inhibitor 1, which support the relevance of the results.

WIDER IMPLICATIONS OF THE FINDINGS: The study increases our understanding of human ovarian function during ovulation, and the publicly available dataset is a valuable resource for future investigations. Suggested upstream regulators and highly differentially expressed genes may be potential pharmaceutical targets in fertility treatment and gynaecology.

STUDY FUNDING/COMPETING INTEREST(S): The study was funded by EU Interreg ÔKS V through ReproUnion (www.reprounion.eu) and by a grant from the Region Zealand Research Foundation. None of the authors have any conflicts of interest to declare.

Key words: ovulation / LH / human / granulosa cells / transcriptomics / oocyte maturation / follicle rupture

Introduction

Ovulation is induced by a massive midcycle surge of gonadotrophins that elicits a cascade of events in granulosa cells (GCs), cumulus cells (CCs) and theca cells (TCs) leading to final maturation of the oocyte, tissue remodelling with expulsion of the oocyte and luteinisation of the follicle cells as they transform into the corpus luteum (CL). These events are central to reproductive success and are coordinated by a crosstalk of signals between the follicle cells and the oocyte that originate in dynamic changes in their transcriptional machinery. In an attempt to understand this interplay, whole transcriptome assessments across the periovulatory interval have previously been performed on GCs or CCs from cows (Assidi et al. 2010; Gilbert et al. 2011; Rao et al. 2011; Christenson et al. 2013), mice (Hernandez-Gonzalez et al. 2006; Carletti and Christenson 2009), horses (Donadeu et al. 2014) and primates (Xu et al. 2011). Owing to considerable interspecies variation (Knight and Glister 2006), these studies do not directly extrapolate to humans. Gaining access to human follicles during ovulation is difficult. Specific subsets of genes have been investigated in women using laparoscopic surgery to excise ovarian tissue at selected time points before and after ovulation induction (OI) (McCord et al. 2012; Al-Alem et al. 2015; Rosewell et al. 2015; Choi et al. 2017b, 2017a). However, whole transcriptome assessments can disclose the collective regulation of all pathways and transcripts involved in the investigated process. We have previously reported a setup that included women undergoing fertility treatment to assess transcriptomic changes between GCs collected by transvaginal follicle puncture before and 36 h after OI in paired samples (Wissing et al. 2014), leaving the actual ovulatory period between the two time points unexplored. Uncovering the transcriptional regulation during the course of ovulation could provide knowledge to improve therapeutic strategies in fertility treatment and to understand infertility related disorders affecting ovarian function. In the present study, we report for the first time the transcriptomic changes and predicted regulators across five different time points throughout the periovulatory period in human GCs.

Materials and Methods

Between September 2016 and March 2018, a prospective cohort study at the Fertility Clinic, Department of Gynaecology and Obstetrics, Holbæk Hospital, Denmark, was conducted as previously described (Poulsen et al. 2019b). Fifty women undergoing IVF/ICSI treatment due to male factor infertility, tubal disease or unexplained infertility were included, and six of these women had been diagnosed with polycystic ovary syndrome. We excluded women with elevated androgens, diseases of the lung, heart, bowel or kidney and dysregulated thyroid disease as well as women above 35 years of age. Women were treated according to a standard antagonist protocol with individually dosed recombinant FSH ($n = 42$; Puregon®, MSD, Denmark) or hMG ($n = 8$; Menopur®, Ferring, Denmark) starting on day 2–3 of the menstrual

cycle. From stimulation day 5–6, a gonadotrophin-releasing hormone (GnRH) antagonist (Ganirelix, 0.25 mg; Fyremadel®, SUN pharma, Netherlands) was administered daily. All hormones were administered s.c. When at least three follicles reached 17 mm in diameter, final maturation of follicles was induced with oocyte retrieval 36 h later. For ethical reasons, only women who had developed more than eight mature follicles at their final control visit before OI were included. As a standard clinical practice to avoid ovarian hyperstimulation syndrome (OHSS), ovulation was induced with recombinant hCG (rhCG; $n = 17$; 6500 IU; Ovitrelle®, Merck Serono, Germany) if a woman developed less than 14 mature follicles, and with GnRH agonist (GnRHa; $n = 33$; buserelin, 0.5 mg; Suprefact®, Sanofi-Aventis, France) if she developed at least 14 follicles ≥ 12 mm or had clinical signs of OHSS. Each woman donated the content of one follicle at one specific time point prior to oocyte retrieval: before OI (group 1, $n = 23$), 12 h (group 2, $n = 10$), 17 h (group 3, $n = 6$) or 32 h after OI (group 4, $n = 11$), and in addition, GCs were isolated from one follicle at oocyte retrieval from all participants ($n = 50$).

Collection of GCs

Follicle aspiration was performed by transvaginal ultrasound-guided follicle puncture with a single lumen needle (Wallace Oocyte Recovery Systems, Smith Medical, Brisbane, Australia). At the first follicle puncture, one easily accessible follicle ≥ 14 mm was aspirated and subsequently double-flushed with flushing medium (ASP®, 10 I00, Vitrolife, Sweden) to increase the number of available GCs. At oocyte retrieval, GCs from the first aspirated follicle containing an oocyte–cumulus complex were used for the study. Double flushing was performed between follicle aspirations to prevent sample carryover.

GCs were isolated from the aspirated follicular fluid and flushing medium with a 100- μ l pipette, while red blood cells and blood clots were avoided. The cells were washed through a 4-well dish containing PBS (AM-9525; Invitrogen, Thermo Fisher, Denmark) and 0.1% polyvinyl alcohol (Sigma-Aldrich, Denmark) and were subsequently transferred to a 0.2-ml cryotube (MicroAmp, Applied Biosystems, Waltham, MA, USA) with minimal fluid, flash frozen in liquid nitrogen and stored at -80°C until further analysis. The GCs were processed within 30 min after follicle aspiration.

Ethical approval

The study setting was a state-financed, public fertility clinic, where treatment is free of charge with a maximum of three complete IVF/ICSI cycles per patient/couple. The participants were included in their first or second IVF/ICSI cycle. They were fully informed of the study including procedures, risks and the involved donation of the content of one follicle, and thereby potentially one oocyte. Participation was voluntary, there was no economic incentive and informed consent was given in accordance with the Helsinki Declaration II and with approval from The Scientific Ethical Committee of Region Zealand, Denmark (SJ-530) and the Danish Data Protection Agency.

Microarray analysis

The Arcturus PicoPure[®] RNA isolation kit (Applied Biosystems, CA, USA) was used to isolate total RNA from GCs according to the manufacturer's instructions. NanoDrop (ThermoFisher, MA, USA) and Bioanalyzer RNA 6000 Pico Kit (Agilent, CA, USA) were used to assess quality and quantity of RNA. The amount of total RNA ranged from 0.19 to 286 ng/μl (Supplementary Table Sla).

Based on RNA concentrations and RNA integrity (RIN) values, RNA was subsequently processed using the Clariom[™] D Pico Assay (Applied Biosystems, Thermo Fisher, USA) according to the manufacturer's protocol (Supplementary Table Sla). The Clariom D Pico Assay can identify >540 000 transcripts from as little as 0.1-ng RNA. The arrays were washed and stained with phycoerythrin-conjugated streptavidin using the Affymetrix Fluidics Station 450, and the arrays were scanned in the Affymetrix GeneArray 3000 7G scanner to generate fluorescent images. Cell intensity files (.CEL files) were generated in the GeneChip Command Console Software (AGCC, Affymetrix, Thermo Fisher, USA).

The raw CEL files were imported into the Transcriptome Analysis Console (TAC, v4.0.1, Applied Biosystems, Thermo Fisher Scientific, MA, USA). After initial quality control analysis, 83 of 100 samples continued to further analysis, representing time points: 0 h ($n = 17$), 12 h ($n = 7$), 17 h ($n = 6$), 32 h ($n = 9$) and 36 h ($n = 44$). Data summarization, quantile normalization, gene summaries and statistical analysis were performed in one analysis flow. Normalization was performed by the signal space transduction—robust multi-array average (SST-RMA) approach (Affymetrix 2019). This SST-RMA normalization is a further development of the well-known RMA approach (Bolstad et al. 2003), designed to optimize fold changes (FCs) that have historically been underestimated by RMA (Affymetrix 2019). An example of how the data output is different between the two normalization approaches is available in Supplementary Table Slk. Direction of change, top differentially expressed genes (DEGs) and bioinformatic results are not affected by choice of normalization approach. The differential expression analysis across time points was setup using ANOVA ebayes comparisons with an advanced random factor for 'patient ID', accounting for the pairing of samples, and an overall false discovery rate (FDR) <0.01. For differential expression between individual time points, an FDR <0.01 combined with a gene level FC <−2 or >2 was considered significant. Furthermore, differential expression between time points was assessed by principal component analysis (PCA) and hierarchical clustering performed in TAC. Included samples with lower RIN values (bottom quarter) were evenly distributed (not outliers) in the PCA plot and among sample signals.

The microarray data was deposited to the Gene Expression Omnibus (<https://www.ncbi.nlm.nih.gov/gds/>, accession number: GSE133868).

Expression of the leukocyte specific marker *PTPRC* (*CD45*) was consistently very low across time points at levels similar to Y-chromosome specific genes, such as *TSPY1* and *DAZ4*, indicating no or low leukocyte contamination with no differences between time points (FDR = 0.076; FC, <1.5). Similarly, large or unequal TC contamination of the GC samples was found unlikely as TC markers, such as *INSL3* and *ACTG2*, showed equally low expression across the time points (data not shown). For definitions of gene symbols, refer to Supplementary Table Sll.

Quantitative reverse transcription-PCR validation of microarray expression

Technical validation of the microarray results was performed using predesigned TaqMan[™] gene expression assays (Thermo Fisher Scientific, MA, USA). Ten genes were selected for validation at specific time points that exemplified their pattern. They were selected based on different expression patterns and FC. At time points 0 h ($n = 17$), 12 h ($n = 7$) and 36 h ($n = 9$), quantitative reverse transcription (qRT)-PCR was performed for *STAR*, *HSD3B2*, *HSD17B1*, *HSD11B1* and *STC1* (product numbers: Hs00264912_m1, Hs00605123_m1, Hs00166219_g1, Hs01547870_m1 and Hs00174970_m1, respectively). At time points 17 h ($n = 5$) and 36 h ($n = 5$), using only paired samples, qRT-PCR was performed for *CYP19A1*, *PTGS2*, *F5*, *ADAMTS1* and *JUN* (product numbers: Hs00903411_m1, Hs00153133_m1, Hs00914120_m1, Hs01547870_m1 and Hs01103582_s1, respectively). Duplicate runs of each sample were prepared with TaqMan[™] Fast Advanced Master Mix (catalog no. 4444557, Thermo Fisher Scientific, MA, USA) according to the manufacturer's instructions. Gene expression was normalized to *GAPDH* (Hs02786624_g1), as this gene has been shown to be highly and stably expressed across different follicle classes (Kristensen et al. 2014) and in the present microarray analysis (differential expression FDR = 0.067). As the GC samples in the present study were not easily obtained, validation in a larger cohort was not possible. For definitions of gene symbols, please refer to Supplementary Table Sll.

Statistical analyses

SPSS (v25, IBM, NY, USA) was used to perform the statistical tests not associated with the microarray analysis. Baseline descriptive parameters between patient groups were compared by a Kruskal–Wallis test and a *post hoc* test with a Bonferroni correction. A P -value <0.05 was considered significant.

To assess differential expression between time points for the PCR validation, the gene levels for time points 17 h and 36 h (*CYP19A1*, *PTGS2*, *F5*, *ADAMTS1*, *JUN*) were log₂ transformed in order to perform a parametrical pairwise Student's *t*-test on five paired samples, as these samples represented five women with two repeated measures. Differential expression of PCR-validated genes for time points 0 h, 12 h and 36 h (*HSD11B1*, *HSD17B1*, *STAR*, *HSD3B2*, *STC1*) were subject to a non-parametric Kruskal–Wallis test as they represented three different groups of women and the sample sizes were unequal.

Pathway and upstream regulator analyses

For the functional analyses, only protein-coding genes were used. The pathways, genes and regulators were assessed in two ways: by genes clusters, and by DEGs between specific time points.

To increase our understanding of the overall regulation of various functions during ovulation, clusters of genes representing distinct expression profiles were produced. Expression values of DEGs, FDR <0.01, were standardized and centred around 0, and a K-nearest neighbours analysis was performed in R (www.r-project.org, Vienna, Austria) based on gene correlations. The gene lists from each of the clusters were imported into Ingenuity Pathway Analysis[®] (IPA, version 49 309 495, QIAGEN Inc., www.qiagenbioinformatics.com/products/ingenuity-pathway-analysis/, (Krämer et al. 2014)), where they were

subject to a core analysis revealing enriched pathways and predicted upstream regulators among the genes. Predicted upstream regulators are known to affect a proportion of genes in a supplied list, and the strength of this prediction is calculated in IPA by a Fisher's exact test. A resulting *P*-value <0.05 was considered significant.

To further explore the details and direction of pathways and regulators (i.e. activation or inhibition), DEGs at 0–12 h, 12–32 h and 32–36 h with an FDR <0.01 and FC >2 or <−2 were analysed with IPA. An activation z-score predicts the activation state of a pathway or regulator using the gene expression patterns in the dataset in relation to what would be expected. A z-score of ≥2 is considered significantly activated and a z-score ≤2 is considered significantly inhibited.

Results

Comparison of baseline descriptive parameters between the study groups showed no difference in examined baseline serum hormone levels, age, total stimulation dosage or number of follicles at the last control ultrasound. However, the group aspirated at 32 h had a slightly lower BMI (*P* = 0.026) and higher serum sex hormone-binding globulin (*P* = 0.038), and the size of the follicles were larger (*P* = 0.0001) compared to those aspirated at 0 h. The 0 h group had a higher of fraction women with male factor infertility (*P* = 0.016) (Supplementary Table S1b).

All qRT-PCR validated genes showed similar expression patterns compared to the microarray analysis and significant regulation of 8 from 10 genes, *P* < 0.05 (Supplementary Fig. S1).

Identified and differentially expressed genes

The microarray analysis identified 135 750 transcripts of which 13 345 were differentially expressed with an overall time point FDR <0.01. The transcripts were distributed in nine different categories (Supplementary Fig. S2). Among DEGs, 9% were unassigned and could represent unknown splice variants. Protein-coding genes represented 58% of DEGs (7699 genes, 'coding' and 'multiple complex' genes) (Supplementary Tables S1a–k). Inter-patient differences and time point differences were the major sources of variation in the dataset with negligible contribution from choice of stimulation and trigger drug (below 3%). Gene expression was at all time points investigated for differences between treatments (FC >2 or <−2 and FDR <0.01), but only GnRH_a versus rhCG triggering at 36 h (*n* = 44 in total) showed a relevant difference with 209 DEGs (with approximately equal up- and downregulation, Supplementary Table S1c).

The PCA analysis showed clear distinction between time points and the pattern followed the experimental design (Fig. 1a). From the number of DEGs between individual time points (Fig. 1b), it was evident that a large number of genes were regulated at 0–12 h (equally up- and downregulated), only 89 DEGs at 12–17 h were found, DEGs at 12–32 h were mainly downregulated (839 from 1014 genes) and DEGs at 32–36 h were almost exclusively upregulated (508 from 578). Differential expression between 32 and 36 h was confirmed by examining only paired samples at 32–36 h (*n* = 9), which also showed almost exclusive upregulation among DEGs (data not shown). Collectively, transcription of genes during ovulation, as shown in the present dataset, could be summarized into two peaks of upregulation at 12 h and 36 h.

DEGs with the highest fold changes are listed in Tables I and II, as they may be of importance to the ovulatory process. DEGs with major upregulation at 0–12 h included *TNFAIP6* (FDR = 2.4E-27), IGF-system regulator *STC1* (FDR = 3.3E-16), *IL7R* (FDR = 5.2E-16), *NTS* (FDR = 9.4E-11) and *ELL2* (FDR = 5.8E-26) (For definitions of gene symbols, refer to Table I).

DEGs with major upregulation at 0–36 h included *HSD11B1* (FDR = 1.4E-45), *ADAMTS9* (FDR = 2.8E-32) *ADAMTS1* (FDR = 6.5E-33). The predominant downregulated gene at 0–36 h was *IGF2* (FDR = 7.5E-28) (For definitions of gene symbols, refer to Table II).

Overall enriched pathways and predicted upstream regulators

Seven gene clusters representing genes of similar regulation across the time points were identified (Supplementary Tables S11a–g). Transcriptional downregulation (cluster 1 and 2) and upregulation with peaks at 12 h (cluster 3), 17 h (cluster 4), 32 h (cluster 5) and 36 h (cluster 6 and 7) were identified. The gene clusters were used as input for assessment of the overall regulation of canonical pathways (Fig. 2) and upstream regulators (Supplementary Fig. S3) across the five investigated time points.

Top enriched canonical pathways for cluster 1 and 2, representing pathways that are shut down following OI, were cell cycle-related pathways with a few related to cell proliferation and DNA repair. Predicted upstream regulators included transcription factors and kinases involved in cell cycle progression (E2F, CDKN, RBL1, TP53, FOXM1) and cell differentiation (MITF, RABL6, HGF, NBRI, ATF6).

Enriched cluster 3 pathways were related to stress signalling, inflammation, protection from oxidative stress and FGF signalling. FSH was predicted to be the most significant upstream regulator, but also LH, oestradiol, cortisol and a number of factors initiating inflammatory cascades (NFκB, TNF, IL1B, TGFB, PDGF, TREM1, IL2 and F2) were predicted regulators.

Cluster 4 pathways were involved in cell-to-cell signalling, JAK/S-TAT signalling, WNT signalling and glycoprotein and lipid synthesis. Upstream regulators included FSH, LH, TGFβ1, some initiating cell proliferation and inflammation (NKX2-3, STAT5B, MDGA2), iron signalling (IREB2, FTMT) and DNA methylation (MECP2, SMYD2), however, with weaker predictions than the preceding clusters.

Cluster 5 pathways were involved in protein synthesis, thrombin signalling (coagulation and angiogenesis), phospholipase C signalling and ERK signalling. The regulators were involved in cell proliferation and differentiation (MYCN), antigen presentation and phagocytosis (FCGR1A, PRDM5) and hypoxia-induced signalling (EPAS1, ARNT).

For both cluster 6 and 7, peaking at 36 h, the top canonical pathways were dominated by cytoskeletal rearrangement and signalling involving the adherence junctions between the cells or to the extracellular matrix (ECM) and inflammation. Upstream regulators for both were PGR, beta-estradiol and EGFR. Predicted upstream regulators for cluster 6 included the nuclear glucocorticoid receptor (NR3C1) and KLF2, known to constrain inflammation. Notably, upstream regulators from cluster 3, such as TNF, TGFβ1, F2, PDGF and MAPK/ERK, were also predicted as regulators for cluster 6 and 7.

For definitions of gene/protein symbols, please refer to Supplementary Table S11.

Table 1 Top regulated genes in human granulosa cells at 0–12 h by fold change.

Gene symbol	Gene name	0 h (log2)	12 h (log2)	Fold change*	FDR P-value
UPREGULATED					
<i>TNFAIP6</i>	Tumor necrosis factor alpha-induced protein 6	3.5	19.8	83774.2	2.4E-27
<i>STC1</i>	Stanniocalcin 1	4.3	19.7	43274.2	3.3E-16
<i>IL7R</i>	Interleukin 7 receptor	3.8	16.2	5535.5	5.2E-16
<i>NTS</i>	Neurotensin	3.7	16.1	5376.6	9.4E-11
<i>ELL2</i>	Elongation factor, RNA polymerase II. 2	6.1	18.5	5334.3	5.8E-26
<i>RUNX1</i>	Runt-related transcription factor 1	5.1	16.8	3296.0	1.1E-25
<i>DUSP6</i>	Dual specificity phosphatase 6	4.2	15.7	2730.6	4.9E-13
<i>AREG</i>	Amphiregulin	4.7	16.1	2727.2	3.7E-15
<i>TM4SF1</i>	Transmembrane 4 L six family member 1	8.5	19.8	2640.1	1.3E-14
<i>FREM2</i>	FRAS1 related extracellular matrix protein 2	4.2	15.2	1978.5	3.5E-26
<i>FGF2</i>	Fibroblast growth factor 2 (basic)	5.6	16.4	1751.5	4.5E-18
<i>RGS2</i>	Regulator of G-protein signaling 2	5.6	16.3	1644.8	3.0E-25
<i>AMDHD1</i>	Amidohydrolase domain containing 1	4.8	15.5	1582.1	3.2E-30
<i>ACPP</i>	Acid phosphatase, Prostate	6.9	17.6	1580.2	2.9E-20
<i>NEBL</i>	Nebulette	4.8	14.9	1131.8	1.6E-24
<i>AHR</i>	Aryl hydrocarbon receptor	6.4	16.5	1130.1	2.1E-11
<i>GFPT2</i>	Glutamine-fructose-6-phosphate transaminase 2	3.4	13.4	1000.1	2.0E-17
<i>SERPINE1</i>	Serpin peptidase inhibitor, Clade E, member 1 (Plasminogen activator inhibitor type 1)	4.0	13.8	869.8	1.5E-11
<i>SLC12A8</i>	Solute carrier family 12, member 8	3.5	13.1	746.3	6.4E-16
<i>SLC7A11</i>	Solute carrier family 7, member 11 (anionic amino acid transporter light chain, xc- system)	4.1	13.6	728.5	2.5E-18
<i>HSD11B1</i>	Hydroxysteroid (11-beta) dehydrogenase 1	4.9	14.4	689.7	1.3E-29
<i>TVP23A</i>	Trans-golgi network vesicle protein 23 homolog A (<i>S. cerevisiae</i>)	5.2	14.5	636.9	1.4E-14
<i>GSTA9P</i>	Glutathione S-transferase alpha 9. pseudogene	4.3	13.7	634.9	1.4E-19
<i>SORD2P</i>	Sorbitol dehydrogenase 2. pseudogene	9.7	18.7	492.2	3.1E-15
<i>PRKX</i>	Protein kinase, X-linked	3.2	12.1	483.0	4.4E-18
<i>SORD</i>	Sorbitol dehydrogenase	9.1	18.0	471.2	1.0E-15
<i>IGFBP3</i>	Insulin like growth factor binding protein 3	3.3	12.1	428.9	4.3E-21
<i>TNFRSF11B</i>	Tumor necrosis factor receptor superfamily, member 11b	4.1	12.6	379.8	8.9E-14
<i>EREG</i>	Epiregulin	3.2	11.8	372.7	8.4E-15
<i>MFHAS1</i>	Malignant fibrous histiocytoma amplified sequence 1	7.0	15.6	372.1	1.1E-24
<i>DIRAS3</i>	DIRAS family, GTP-binding RAS-like 3	3.7	12.2	352.6	3.9E-10
<i>MRO</i>	Maestro	9.5	17.6	278.3	6.9E-09
<i>BIRC3</i>	Baculoviral IAP repeat containing 3	4.9	13.0	274.3	6.1E-16
<i>TNFAIP3</i>	Tumor necrosis factor alpha-induced protein 3	8.8	16.9	273.7	3.2E-17
<i>ARID5B</i>	AT rich interactive domain 5B (MRF1-like)	6.1	14.1	246.8	6.7E-13
<i>SEMA6A</i>	Sema domain, Transmembrane domain (TM), and cytoplasmic domain, (semaphorin) 6A	5.4	13.2	233.5	1.6E-14
<i>PTH1LH</i>	Parathyroid hormone-like hormone	3.8	11.7	232.5	1.5E-11
<i>FAM46A</i>	Family with sequence similarity 46. member A	5.2	13.0	214.8	1.5E-15
<i>RHOU</i>	Ras homolog family member U	4.9	12.5	189.1	4.3E-21
<i>E2F7</i>	E2F transcription factor 7	8.5	16.0	183.7	1.1E-12
<i>RAPH1</i>	Ras association (RalGDS/AF-6) and pleckstrin homology domains 1	5.3	12.8	177.2	3.0E-13
<i>SLC35E3</i>	Solute carrier family 35, member E3	9.1	16.4	161.9	4.6E-07
<i>TSC22D1</i>	TSC22 domain family, Member 1	7.5	14.8	158.1	9.9E-16
<i>LXN</i>	Latexin	7.1	14.4	153.9	4.2E-05
<i>OSMR</i>	Oncostatin M receptor	4.6	11.8	151.7	3.9E-15

Continued

Table I Continued.

Gene symbol	Gene name	0 h (log2)	12 h (log2)	Fold change*	FDR P-value
DOWNREGULATED					
<i>PLEKHH1</i>	Pleckstrin homology domain containing, Family H (with MyTH4 domain) member 1	15.5	7.0	-353.5	2.1E-08
<i>ACSM3</i>	Acyl-CoA synthetase medium-chain family member 3	15.7	7.8	-245.0	1.1E-03
<i>HIST1H2AG</i>	Histone cluster 1, H2ag	15.8	8.1	-208.7	3.2E-05
<i>SLC7A8</i>	Solute carrier family 7, member 8 (amino acid transporter light chain, L system)	16.4	8.7	-206.4	1.7E-07
<i>FSCN1</i>	Fascin actin-bundling protein 1	12.7	5.3	-177.7	2.7E-08

The table highlights genes whose expression levels changed the most during ovulation.

*The data were normalized using the signal space transduction—robust multi-array average (SST-RMA) approach (Affymetrix 2019) that increases fold changes compared to standard RMA, with a similar significance level. FDR: false discovery rate.

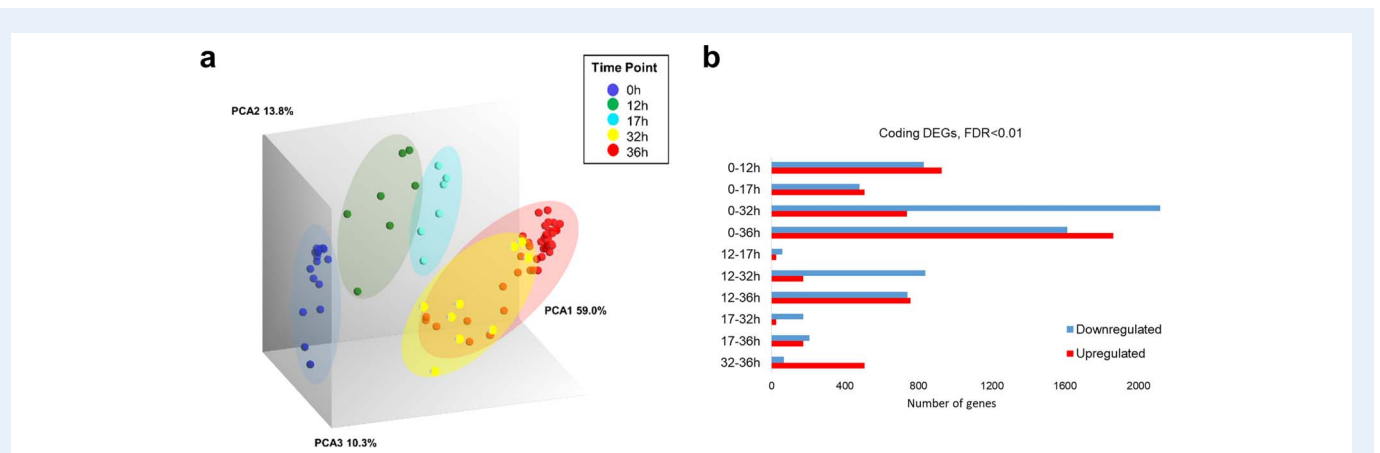


Figure 1 Behaviour of differentially expressed genes in human granulosa cells. (a) Principal component analysis plot. The pattern followed the experimental design with the largest difference in granulosa cell (GC) from 0 to 36 h samples, and a closer relation between 12 h and 17 h samples as well as 32 h and 36 h samples. There was a clear distinction between time points 0–32 h, while some overlap was found between samples at 32 h and 36 h. However, the majority of 36 h samples was separated from the 32 h samples. (b) Number of differentially expressed genes (DEGs) between individual time points. PCA: principal component analysis, FDR: false discovery rate.

Regulators and pathways among DEGs at 0–12 h and 32–36 h

As the transcriptional changes were dominated by upregulation peaks at 12 h and 36 h, we analysed DEGs at 0–12 h and 32–36 h separately to obtain a prediction of activation or inhibition of pathways and regulators from IPA. The upstream regulator analysis for these gene sets revealed that many of the same factors drive the changes at 0–12 h and 32–36 h (Fig. 3, panel a and b) including TGFBI, TNF, IL6, F2, EGF, HGF, CSF2, FGF2, NFKB and STAT3, among others. Conversely, the same factors were predicted as inhibited for DEGs at 12–32 h, due to downregulation of numerous genes at 12–32 h (Supplementary Tables S1d–f). FSH and LH, the physiological activators of ovulation, were among the predicted activators of DEGs at 0–12 h and were also predicted as strong regulators in the cluster analyses. IPA generated two networks by known interactions and predictions, which suggested how FSH and LH may affect other upstream regulators in the dataset. The networks induced by these factors are of special interest, as they may explain how the ovulation cascade is initiated (Fig. 4).

The predicted activated canonical pathways between 0 and 12 h were inflammation, immune and acute response related and covered the central inflammation related pathways such as JAK/STAT signalling, MAPK/p38 signalling and NFKB signalling (Table III). The predicted inhibited pathways included primarily, as for the clusters, cell cycle regulation, cellular development and cancer-related pathways.

The activated pathways between 32 and 36 h included phospholipase C signalling and a number of pathways involved in cell migration and actin cytoskeleton dynamics, for example ephrin receptor signalling, rho signalling and integrin signalling. In addition, chemokine signalling (e.g. IL8 and CXCR4), thrombin signalling (i.e. blood coagulation and adhesion) and inflammatory pathways (IL6 and p38/MAPK) were enriched. The only definitively inhibited pathway during this period was Rho GDI (i.e. inhibition of cytoskeletal rearrangements and cell motility) (Table IV).

Inflammation

To further investigate the inflammation-related events, a list of 2895 genes related to inflammation, innate immunity and wound healing

Table II Top regulated genes in human granulosa cells at 0–36 h by fold change.

Gene symbol	Description	0 h (log2)	36 h (log2)	Fold change*	FDR P-value
UPREGULATED					
<i>HSD11B1</i>	Hydroxysteroid (11-beta) dehydrogenase 1	4.9	19.4	22646.8	1.4E-45
<i>ADAMTS9</i>	ADAM metalloproteinase with thrombospondin type 1 motif 9	3.9	17.5	12293.7	2.8E-32
<i>ADAMTS1</i>	ADAM metalloproteinase with thrombospondin type 1 motif 1	3.4	16.7	10192.9	6.5E-33
<i>PLIN2</i>	Perilipin 2	4.5	16.0	2854.7	9.2E-30
<i>TM4SF1</i>	Transmembrane 4 L six family member 1	8.5	19.9	2718.4	9.8E-27
<i>ANKRD22</i>	Ankyrin repeat domain 22	3.9	15.1	2417.1	1.6E-28
<i>DCN</i>	Decorin	4.6	15.8	2237.8	1.7E-17
<i>NTS</i>	Neurotensin	3.7	14.8	2127.7	4.6E-18
<i>SERPINE1</i>	Serpin peptidase inhibitor, clade E1 (plasminogen activator inhibitor type 1)	4.0	14.7	1672.6	7.5E-28
<i>DUSP6</i>	Dual specificity phosphatase 6	4.2	14.9	1556.9	9.4E-26
<i>LUM</i>	Lumican	3.2	13.3	1104.7	3.2E-14
<i>RUNX1</i>	Runt-related transcription factor 1	5.1	15.1	1029.7	1.1E-36
<i>FBXO32</i>	F-box protein 32	3.4	13.3	982.9	1.8E-29
<i>ERRFI1</i>	ERBB receptor feedback inhibitor 1	5.7	15.2	754.8	3.8E-24
<i>RGS2</i>	Regulator of G-protein signaling 2	5.6	15.1	735.9	9.5E-38
<i>CPM</i>	Carboxypeptidase M	5.3	14.8	729.9	8.0E-23
<i>PRKX</i>	Protein kinase, X-linked	3.2	12.6	673.8	1.7E-35
<i>SLCO2A1</i>	Solute carrier organic anion transporter family, Member 2A1	3.0	12.3	642.3	1.7E-28
<i>TIMP1</i>	TIMP metalloproteinase inhibitor 1	9.4	18.6	611.0	1.4E-45
<i>TECRL</i>	Trans-2,3-enoyl-CoA reductase-like	2.9	12.1	602.6	6.3E-22
<i>SAT1</i>	Spermidine/spermine N1-acetyltransferase 1	8.9	18.1	564.9	2.4E-37
<i>SEMA3A</i>	Sema domain, Immunoglobulin domain (Ig), short basic domain, Secreted, (semaphorin) 3A	6.8	15.9	547.0	7.5E-18
<i>RUNX2</i>	Runt-related transcription factor 2	4.8	13.7	485.1	1.3E-28
<i>PKP2</i>	Plakophilin 2	5.4	14.1	442.7	8.1E-27
<i>AREG</i>	Amphiregulin	4.7	13.3	407.2	1.2E-21
<i>ELL2</i>	Elongation factor, RNA polymerase II, 2	6.1	14.6	360.4	2.8E-33
<i>ABCC3</i>	ATP binding cassette subfamily C member 3	3.3	11.7	349.6	6.1E-25
<i>CD24</i>	CD24 molecule	4.9	13.2	309.5	2.3E-29
<i>EFEMP1</i>	EGF containing fibulin-like extracellular matrix protein 1	3.3	11.5	303.4	1.8E-31
<i>FABP6</i>	Fatty acid binding protein 6, ileal	3.9	12.0	278.8	1.1E-32
<i>FNI</i>	Fibronectin 1	4.4	12.5	264.6	1.5E-19
<i>ANPEP</i>	Alanine (membrane) aminopeptidase	3.8	11.8	245.5	3.4E-17
<i>RHOU</i>	Ras homolog family member U	4.9	12.8	231.0	9.9E-39
<i>FLRT2</i>	Fibronectin leucine rich transmembrane protein 2	3.1	10.7	199.1	3.0E-18
<i>IRAK3</i>	Interleukin 1 receptor associated kinase 3; microRNA 6502	3.1	10.7	196.8	1.9E-29
<i>PTGS2</i>	Prostaglandin-endoperoxide synthase 2 (prostaglandin G/H synthase and cyclooxygenase)	4.2	11.7	182.4	1.8E-21
<i>SLC6A6</i>	Solute carrier family 6 (neurotransmitter transporter), member 6	5.8	13.2	171.0	1.1E-19
DOWNREGULATED					
<i>IGF2</i>	Insulin-like growth factor 2	16.4	6.4	-978.8	7.5E-28
<i>HIST1H2AG</i>	Histone cluster 1, H2ag	15.8	6.1	-851.7	1.2E-19
<i>CYP17A1</i>	Cytochrome P450, family 17, subfamily A, polypeptide 1	14.1	5.0	-521.2	1.6E-17
<i>UBE2C</i>	Ubiquitin-conjugating enzyme E2C	12.9	4.0	-506.8	7.5E-27
<i>LRP8</i>	LDL receptor related protein 8	15.5	6.6	-466.4	2.4E-23
<i>UBE2T</i>	Ubiquitin conjugating enzyme E2T	13.1	4.6	-371.9	4.1E-24
<i>HIST1H2BM</i>	Histone cluster 1, H2bm	15.2	7.3	-231.2	3.9E-13

Continued

Table II Continued.

Gene symbol	Description	0 h (log2)	36 h (log2)	Fold change*	FDR P-value
<i>CSNK1G1</i>	Casein kinase I, gamma 1	11.7	3.8	-230.3	6.9E-25
<i>MKI67</i>	Marker of proliferation Ki-67	11.9	4.0	-228.1	1.2E-31
<i>FSCN1</i>	Fascin actin-bundling protein 1	12.7	5.2	-182.0	2.9E-19
<i>GSTA1</i>	Glutathione S-transferase alpha 1	16.8	9.3	-174.2	3.9E-22
<i>CMTM8</i>	CKLF-like MARVEL transmembrane domain containing 8	16.5	9.1	-168.5	1.2E-15
<i>PRCI</i>	Protein regulator of cytokinesis 1	12.9	5.5	-166.4	1.6E-32

The table highlights genes whose expression levels changed the most during ovulation.

*The data were normalized using the SST-RMA approach (Affymetrix 2019) that increases fold changes compared to standard RMA, with a similar significance level.

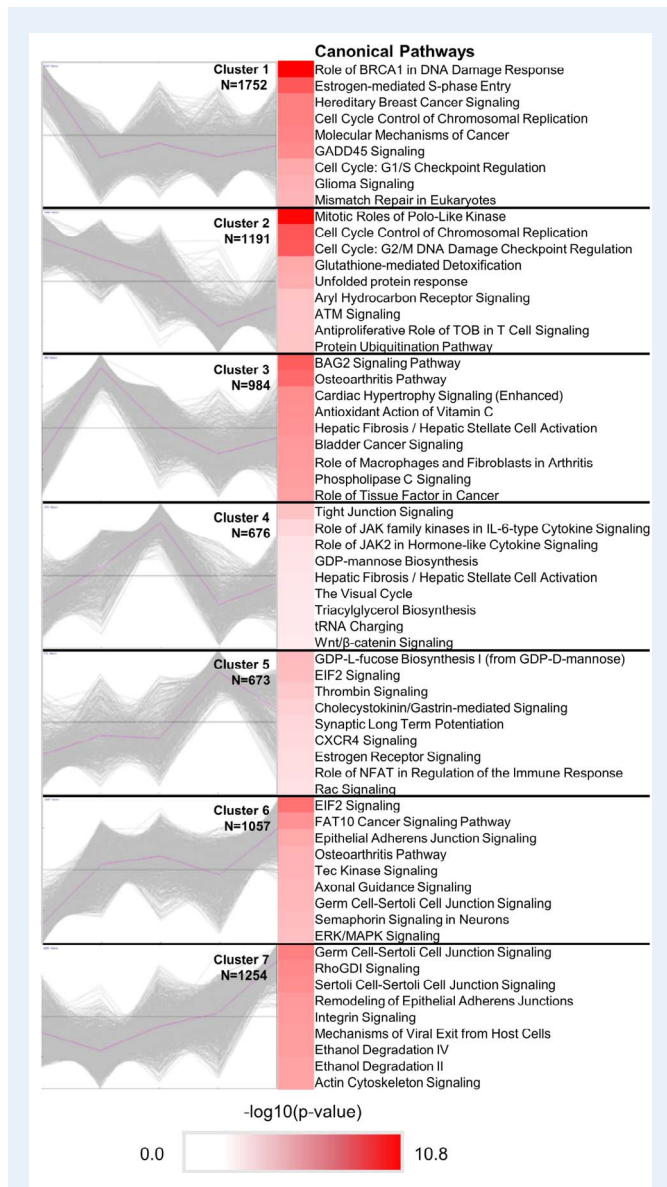


Figure 2 Predicted enriched canonical pathways for seven clusters. The top predicted pathways are depicted. The significance of the prediction is depicted as colour intensity.

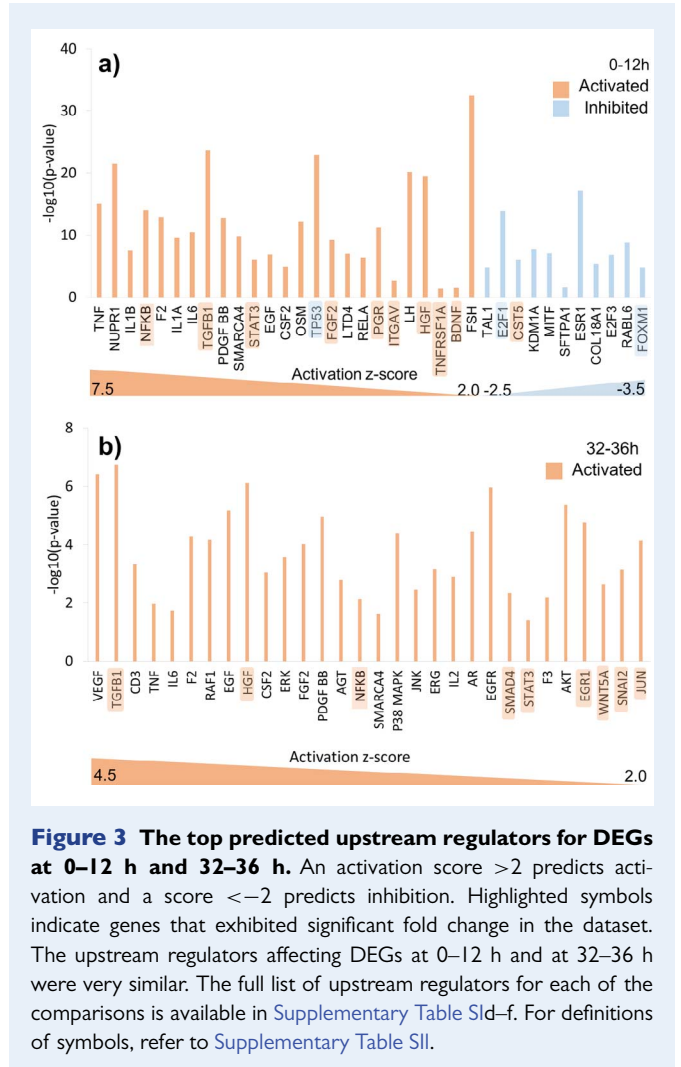


Figure 3 The top predicted upstream regulators for DEGs at 0–12 h and 32–36 h. An activation score >2 predicts activation and a score <–2 predicts inhibition. Highlighted symbols indicate genes that exhibited significant fold change in the dataset. The upstream regulators affecting DEGs at 0–12 h and at 32–36 h were very similar. The full list of upstream regulators for each of the comparisons is available in Supplementary Table S4d–f. For definitions of symbols, refer to Supplementary Table S11.

were generated from the National Center for Biotechnology Information gene site (www.ncbi.nlm.nih.gov/gene, date 16-07-2019) (Brown et al. 2015) (Supplementary Table S1g). The genes were predominant in three clusters: cluster 3, 6 and 7, where they represented 12.7%, 14.8% and 15.0% of the DEGs, respectively. The three gene sets had many pathways in common, especially cluster 3 and 6 were

Table III Top enriched pathways among differentially expressed genes in human granulosa cells at 0–12 h.

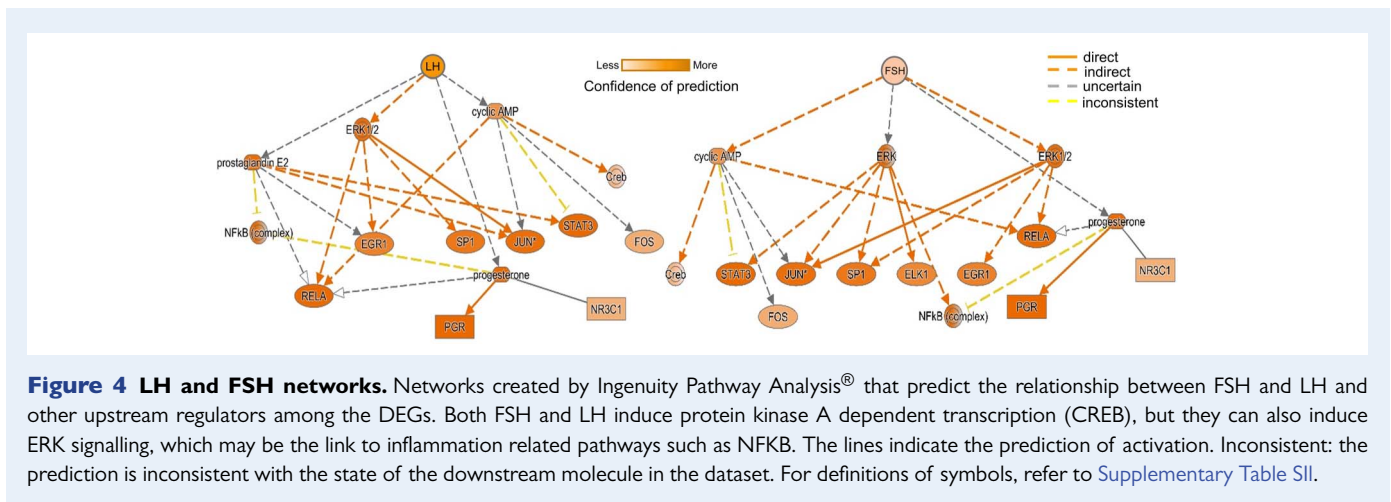
Ingenuity canonical pathways	P-value	Activation z-score
Predicted activation		
Acute Phase Response Signalling	0.0021	3.77
STAT3 Pathway	0.0009	2.84
PFKFB4 Signalling Pathway	0.0005	2.53
Phospholipase C Signalling	0.0245	2.52
IL-6 Signalling	0.0062	2.50
Role of IL-17F in Allergic Inflammatory Airway Diseases	0.0437	2.45
NRF2-mediated Oxidative Stress Response	0.0003	2.32
p38 MAPK Signalling	0.0178	2.31
Bladder Cancer Signalling	0.0076	2.24
FAT10 Cancer Signalling Pathway	0.0078	2.12
Colorectal Cancer Metastasis Signalling	0.0043	1.88
ERK5 Signalling	0.0018	1.73
FGF Signalling	0.0074	1.73
PI3K/AKT Signalling	0.0372	1.73
Cardiac Hypertrophy Signalling (Enhanced)	0.0002	1.70
Opioid Signalling Pathway	0.0018	1.51
NF-KB Activation by Viruses	0.0158	1.51
NF-KB Signalling	0.0331	1.41
Signalling by Rho Family GTPases	0.0030	1.28
Tec Kinase Signalling	0.0275	1.16
TVWAK Signalling	0.0049	1.13
TNFR1 Signalling	0.0100	1.13
Acute Myeloid Leukemia Signalling	0.0251	1.13
Calcium Signalling	0.0076	1.07
Ephrin Receptor Signalling	0.0347	1.07
ERK/MAPK Signalling	0.0013	1.04
Osteoarthritis Pathway	0.0003	1.00
Histidine Degradation III	0.0009	1.00
TNFR2 Signalling	0.0339	1.00
CDP-diacylglycerol Biosynthesis I	0.0347	1.00
Phosphatidylglycerol Biosynthesis II (Non-plastidic)	0.0479	1.00
4-1BB Signalling in T Lymphocytes	0.0501	1.00
Predicted inhibition		
Sumoylation Pathway	0.0018	-2.11
ATM Signalling	0.0030	-2.11
Pyrimidine Deoxyribonucleotides <i>De Novo</i> Biosynthesis I	0.0479	-2.00
RhoGDI Signalling	0.0178	-1.60
Cell Cycle: G2/M DNA Damage Checkpoint Regulation	0.0034	-1.41
BAG2 Signalling Pathway	0.0045	-1.41
Antioxidant Action of Vitamin C	0.0282	-1.41
Apoptosis Signalling	0.0035	-1.39
Role of BRCA1 in DNA Damage Response	0.0001	-1.27
Small Cell Lung Cancer Signalling	0.0018	-1.13
UVB-Induced MAPK Signalling	0.0017	-1.00
Ovarian Cancer Signalling	0.0155	-1.00
SPINK1 General Cancer Pathway	0.0158	-1.00
Paxillin Signalling	0.0389	-1.00

Output from Ingenuity® pathway analysis. The *P*-value represents the significance of the overlap between genes in the canonical pathways and the genes in the dataset. The activation z-score is based on relationship between the expected and observed change of the involved genes in the dataset. Positive z-score suggests activation, and a negative score inhibition, but only a z-score ≥ 2 is significant for activation and ≤ -2 is significant for inhibition.

Table IV Top enriched pathways among differentially expressed genes in human granulosa cells at 32–36 h.

Ingenuity canonical pathways	P-value	Activation z-score
Predicted activation		
Cardiac Hypertrophy Signaling (Enhanced)	0.0021	4.24
Superpathway of Inositol Phosphate Compounds	0.0115	3.00
Colorectal Cancer Metastasis Signaling	0.0204	3.00
Signaling by Rho Family GTPases	0.0023	2.83
IL-8 Signaling	0.0132	2.83
Phospholipase C Signaling	0.0468	2.83
Integrin Signaling	0.0006	2.71
I4–3–3-mediated Signaling	0.0000	2.65
Cholecystokinin/Gastrin-mediated Signaling	0.0071	2.65
G Beta Gamma Signaling	0.0089	2.65
CXCR4 Signaling	0.0138	2.65
Ephrin Receptor Signaling	0.0209	2.65
Actin Cytoskeleton Signaling	0.0009	2.53
HGF Signaling	0.0013	2.45
p38 MAPK Signaling	0.0074	2.45
Rac Signaling	0.0195	2.45
IL-6 Signaling	0.0339	2.45
Thrombin Signaling	0.0417	2.45
Osteoarthritis Pathway	0.0065	2.33
Ceramide Signaling	0.0071	2.24
Actin Nucleation by ARP-WASP Complex	0.0107	2.24
fMLP Signaling in Neutrophils	0.0234	2.24
Androgen Signaling	0.0011	2.00
UVC-Induced MAPK Signaling	0.0158	2.00
Regulation of Actin-based Motility by Rho	0.0263	2.00
Tec Kinase Signaling	0.0347	2.00
Cardiac Hypertrophy Signaling	0.0006	1.73
ERK/MAPK Signaling	0.0012	1.67
HMGB1 Signaling	0.0316	1.63
ILK Signaling	0.0000	1.60
Production of Nitric Oxide and Reactive Oxygen Species in Macrophages	0.0263	1.41
Huntington's Disease Signaling	0.0056	1.34
Chemokine Signaling	0.0158	1.34
P2Y Purigenic Receptor Signaling Pathway	0.0347	1.34
Colanic Acid Building Blocks Biosynthesis	0.0001	1.00
Regulation of Cellular Mechanics by Calpain Protease	0.0013	1.00
Gαi Signaling	0.0324	1.00
Predicted inhibition		
RhoGDI Signaling	0.0006	-2.12
HIPPO signaling	0.0054	-1.34
PPAR Signaling	0.0032	-1.13

Output from Ingenuity® pathway analysis. The *P*-value represents the significance of the overlap between genes in the canonical pathways and the genes in the dataset. The activation z-score is based on relationship between the expected and observed change of the involved genes in the dataset. Positive z-score suggests activation, and a negative score inhibition, but only a z-score ≥ 2 is significant for activation and ≤ -2 is significant for inhibition.



almost similar regarding functions and pathways, while cluster 7 represented other inflammation related pathways ([Supplementary Fig. S4](#)). The results showed that while an acute inflammatory response was initiated immediately after OI, the effector functions of inflammation, such as vasodilation, angiogenesis, coagulation, chemotaxis and tissue remodelling, were primarily active just prior to follicle rupture.

Tissue remodelling

Extracellular remodelling as part of cumulus expansion, follicle rupture and follicular-luteal transition was explored by a combined gene list of 384 genes obtained from Molecular Signatures Database (MsigDB, <http://software.broadinstitute.org/gsea/index.jsp>, Broad Institute, San Diego, CA, USA ([Subramanian et al. 2005](#))) representing ECM organisation ([Supplementary Table SIh](#)). Of these, 127 were DEGs. The top 31 DEGs (FDR, <1.0E-13) were analysed using hierarchical clustering in TAC to indicate similar regulation or similar function ([Fig. 5](#)).

A large group peaked at 36 h, including the protease inhibitor *TIMP1* (FDR = 1.8E-44) and proteases *ADAMTS1* (FDR = 1.6E-29) and *ADAMTS9* (2.53E-29). *TIMP1* clustered with *APP* and *ECE1*. *ADAMTS1* and *ADAMTS9* clustered with the plasminogen activator inhibitor *SERPINE1*, the small proteoglycans *DCN* and *LUM* and an actin filament binding protein (*ANXA2*).

A specific midovulatory function was indicated for *TNFAIP6* (FDR = 3.3E-32), which is known to be involved in cumulus expansion. It clustered with *COL4A1*, *MMP10*, *ADAM12*, *FGF2*, *FGG* and *ITGA6*. For definitions of gene symbols, refer to [Supplementary Table SII](#).

GC contributions to oocyte maturation

Factors contributing to meiotic resumption were assessed using a compiled list of tentative maturational factors working in GCs or CCs obtained from the literature, as reviewed in ([Coticchio et al. 2015](#); [Richani and Gilchrist 2018](#)) ([Supplementary Table SII](#)). Of these, 23 were DEGs in the present dataset ([Fig. 6](#)). Of the EGF ligand encoding genes, *AREG* was predominant with a massive upregulation at 0–12 h (FDR = 6.4E-19), but *EREG*, *BTC* and *ADAM17*, which releases the membrane bound EGF ligands to the soluble extracellular form, all followed a similar pattern, peaking at 12 h. *NPR2* decreased immediately

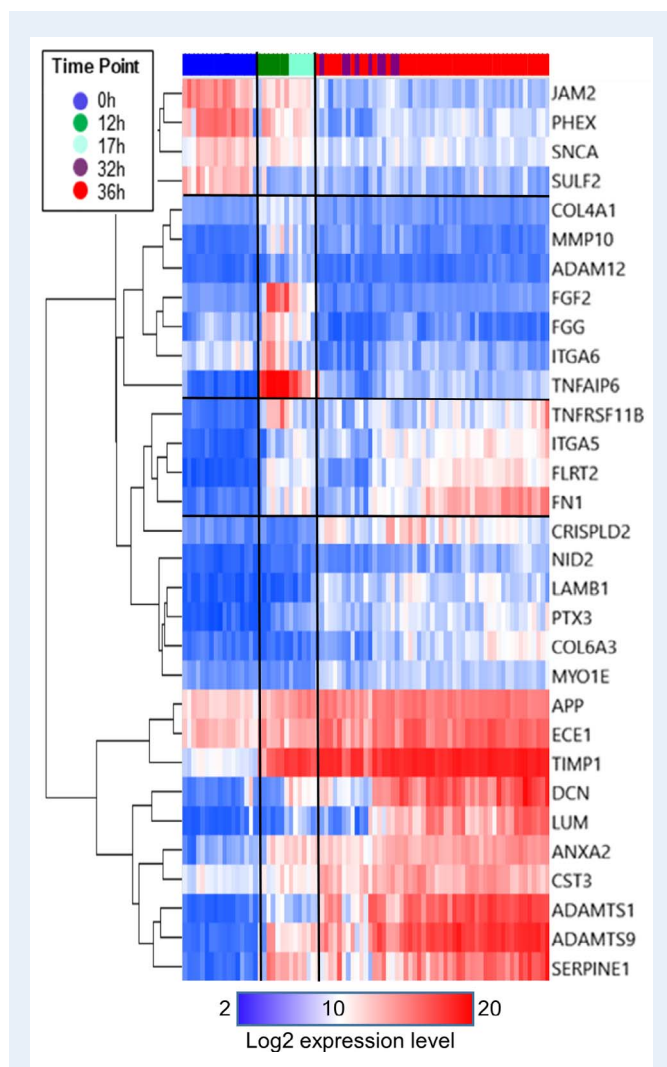
after OI (FDR = 0.0005), as did the gene encoding estrogen receptor beta (*ESR2*, FDR = 1.3E-8). Two gap junction protein-encoding genes, *GJC1* and *GJA1*, were downregulated after 0 h or after 12 h, respectively. *NPPC* and *NRG1* were not significantly regulated. For definitions of gene symbols, refer to [Supplementary Table SIj](#).

Discussion

This study assessed dynamic changes in the human GC transcriptome during ovulation. GCs were obtained from consenting women undergoing fertility treatment, where one follicle puncture was performed at one of five selected time points during the periovulatory period prior to oocyte retrieval (before or 12 h, 17 h or 32 h after OI), and a second paired sample of GCs was collected at oocyte retrieval (36 h after OI). The resulting dataset provided the first, unique insight into the collective time course of events during ovulation in women. Two peaks of transcriptional upregulation at 12 h and 36 h after OI dominated the picture and the most central upstream regulators predicted to drive these changes were, besides LH and FSH, *TGFB1*, *TNF*, *NFKB*, *F2*, *FGF2*, *IL1* and *cortisol*.

Transcriptional upregulation between 0 and 12 h resembled an acute phase response involving pathways centred around classic innate immune signalling cascades, such as *NFKB*, *JAK/STAT* and *MAPK/p38/ERK*, also including *TGFB*, *FGF* and phospholipase C signalling. The second wave of upregulation took place just before the time of follicle rupture, where a higher proportion of enriched pathways were involved in the effector functions of inflammation, such as chemotaxis, prostaglandin synthesis and coagulation, besides pathways related to cell migration and cell–ECM communication.

The regulation of inflammation-related genes during ovulation confirms previous findings. Lawrence Espey was the first to propose the similarity between ovulation and inflammation ([Espey 1980](#)), which was later supported by, for example, microarray studies of periovulatory GCs or CCs in mice ([Hernandez-Gonzalez et al. 2006](#)), cows ([Rao et al. 2011](#)) and rhesus monkeys ([Xu et al. 2011](#)), and a recent review reached a similar conclusion ([Duffy et al. 2019](#)). Using a microarray dataset from GCs collected before OI and 36 h after, we have recently suggested that GCs possess the ability to execute a complete innate immune system-regulated inflammatory reaction during ovula-



tion (Poulsen et al. 2019a). These pronounced characteristics point towards a third 'ovulatory' phenotype of GCs, which is related to that of immune cells (Poulsen et al. 2019a). Cortisol, produced by *HSD11B1*, acting through the glucocorticoid receptor (*NR3C1*), was among the principal suggested upstream regulators. Both *HSD11B1* and *NR3C1* were highly upregulated between 0 and 12 h and stayed elevated, which indicate that the follicle implements the tools to contain and downregulate the inflammatory reaction in parallel with upregulation of inflammatory mediators.

The present study did not reveal the exact connection between the gonadotrophin surge and inflammation. As LH and FSH induce the ovulatory cascade, the logical explanation is that they induce the release of early response upstream regulators identified in the present study, such as *IL1*, *IL6* and *TNF*. These may be ready for immediate release from GCs upon stimulation, or there may be an interplay with the cells surrounding the follicle (i.e. TCs and leukocytes). The network downstream of FSH and LH showed predominantly two modes of

activation: activation of PKA through cAMP and activation of ERK. The cAMP pathway is the most well-described pathway employed by these receptors, which has been linked to resumption of oocyte meiosis (Richani and Gilchrist 2018). However, studies of human GC cell cultures have determined that approximately one-fourth of LH and FSH regulated genes are altered by cAMP-independent mechanisms (Amsterdam 2003). ERK1/2 can be activated by the LHCG receptor or FSH receptor either directly or through the phospholipase C pathway (Ascoli et al. 2002; Gloaguen et al. 2011), and ERK is capable of activating, for example, the inflammatory mediator and upstream regulator NFkB, whose subunits were upregulated immediately after OI in the present study. Enrichment of phospholipase C signalling among DEGs at 0–12 h and 32–36 h in the present study support the use of this pathway. In addition, the FSH and LH networks also suggested an ovulatory role for signalling by progesterone through its receptor (PGR), as *PGR* levels increased massively at 0–12 h and decreased after 17 h. Signalling through this receptor has previously been implicated in follicular rupture through protease activation in mice and primates (Robker et al. 2000; Kim et al. 2009; Bishop et al. 2016) and *PTGS2* induction in humans (Choi et al. 2017b)—pathways that are also integrated in classic inflammation.

The present GC analysis gave a clue to the relevance and timed regulation of the mechanisms connecting the gonadotrophin surge to resumption of meiosis, which have been extensively studied, especially in rodents (Coticchio et al. 2015; Richani and Gilchrist 2018). As the present study is purely descriptive, causation cannot be determined, but the stepwise regulation of genes may indicate the succession of events. We found significant regulation of many of the involved genes (Fig. 6). For example, *AREG* and *EREG* were vastly upregulated at between 0 and 12 h, whereas *NPR2* was significantly downregulated in the same period (Fig. 6), which indicates that oocyte meiotic resumption is induced as one of the first events during the ovulatory process. This is in agreement with a report concluding that germinal vesicle breakdown takes place approximately 15 h after OI (Bomse-Helmreich et al. 1987). NPPC/NPR2 signalling has been found to be enhanced by the estrogen receptor in mice (Zhang et al. 2011) and in humans (Liu et al. 2017), which is in accordance with an *ESR2* decrease at 0–12 h in the present study. Furthermore, we found downregulation of *GJA1* and *GJC1*, encoding gap junction proteins connexin 43 and 45, respectively, which have been found to co-localize in rat GCs (Okuma et al. 1996). Our finding is consistent with the theory that closure of gap junctions facilitates resumption of meiosis by halting the influx of cGMP to the oocyte during ovulation (Norris et al. 2008; Coticchio et al. 2015) and shows that downregulation of both connexin 43 and 45 may contribute to this in human GCs. The EGF cascade has been suggested to autoenhance by induction of prostaglandin E2 (*PGE2*) production (Shimada et al. 2006; Fang et al. 2013; Richani and Gilchrist 2018). However, the present data showed that *PTGES*, the final enzyme in *PGE2* synthesis, is not upregulated until after 17 h, which is potentially too late for an effect on meiotic resumption. However, a second upregulation of the EGF ligands takes place at 32–36 h in the present study, which may be a wave induced by *PGE2*. The EGF ligands are active during wound healing (Zaiss et al. 2015), and the 32–36 h upregulation may therefore indicate that they have a second role in follicle transformation.

The temporal regulation of ECM remodelling factors in GCs (Fig. 5) suggested that genes that peaked mid-ovulation may be involved in

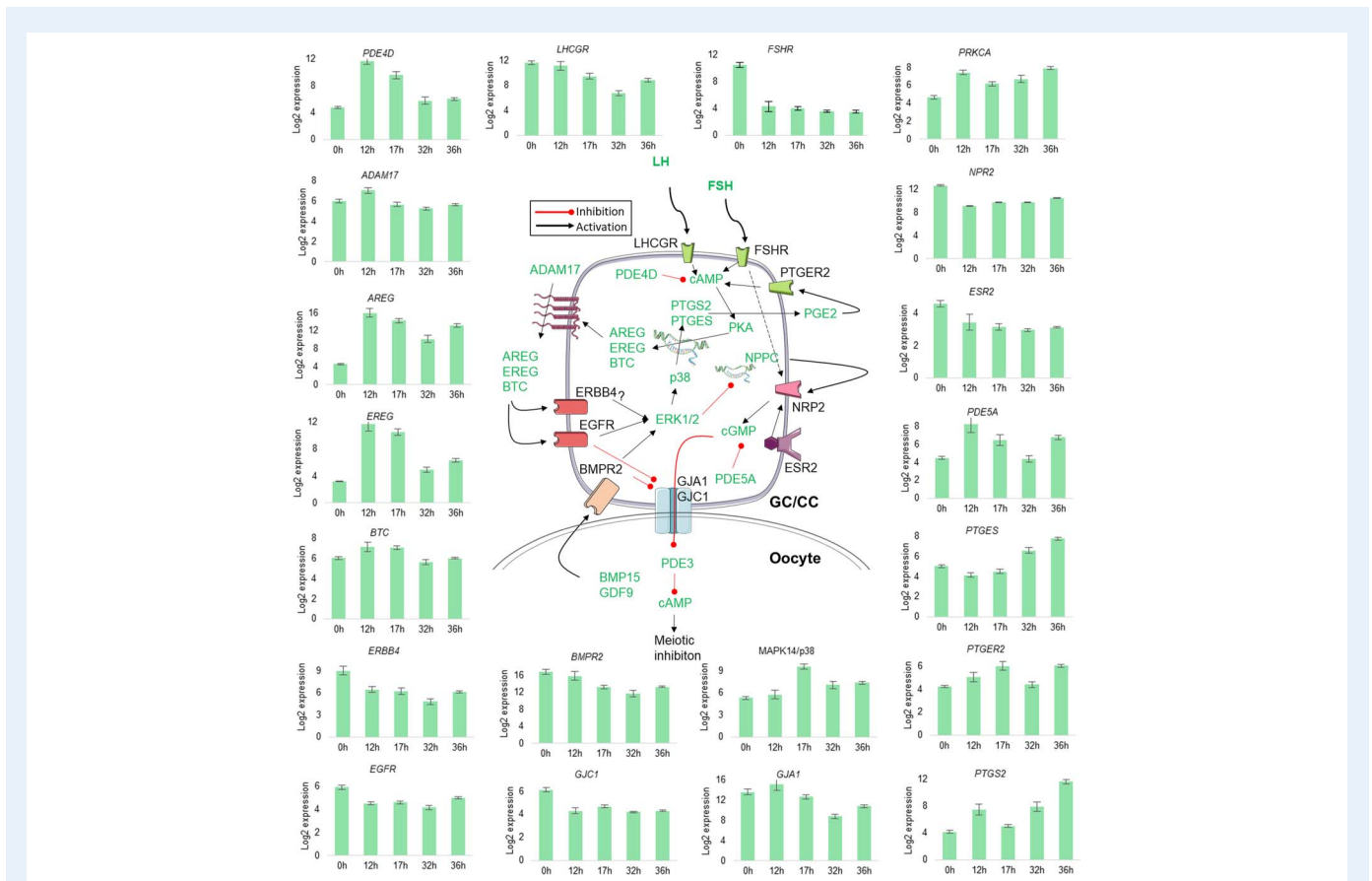


Figure 6 Oocyte maturation. Model depicting factors in GCs that were previously described as being involved in resumption of meiotic maturation, as reviewed in (Coticchio et al. 2015; Richani and Gilchrist 2018). The bar charts depict the results from the present study with mean (\log_2) sample signals and \pm SEM error bars. LH induces cAMP production that causes upregulation of the EGF family ligands AREG, EREG and BTC. They are initially anchored to the cell membrane but released by ADAM17. They subsequently bind to the EGF receptors. This induces an ERK signalling cascade, which inhibits transcription of NPPC. NPPC is a ligand, which upon binding to its receptor (NPR2) causes cGMP production. cGMP is responsible for sustaining oocyte cAMP levels through inhibition of the cAMP degrading enzyme PDE3. cGMP diffuses through gap junctions, and closure of these may facilitate decreased oocyte cAMP. A crosstalk between oocyte and GC involves the bone morphogenic protein receptor (BMPR2), which synergises with the EGF ligand cascade. The oestrogen receptor (ESR2) is involved in transcription of NPR2 to sustain meiotic inhibition prior to ovulation induction. PDE5A degrades cGMP. The GCs are believed to autoenhance the EGF cascade by p38 induction of prostaglandin E_2 (PGE_2)-synthesizing enzymes. PGE_2 binds to its receptor in GC to induce cAMP production. For definitions of symbols, refer to Supplementary Table SII.

cumulus expansion as they cluster with *TNFAIP6*, a well-established factor in this process (Baranova et al. 2014). Another gene in this cluster, *FGF2*, has recently been reported to be regulated by oocyte secreted factors, to increase oocyte meiotic maturation, and affect cumulus expansion (Barros et al. 2019). The collagen *COL4A1* and the integrin *ITGA6* have been associated with cumulus expansion in cattle (Sutovsky et al. 1995). The co-regulated genes, *MMP10*, *FGG* and *ADAM12*, are thus potentially also implicated in cumulus expansion. It was surprising to find that *PTX3* peaked at 36 h and not mid-ovulation, as its protein product has been shown to co-operate with *TNFAIP6* to ensure stable cumulus expansion (Baranova et al. 2014). Likewise, the gene encoding the hyaluronan synthesizing enzyme (*HAS2*) only exhibited a moderate increase at 0–36 h ($FC = 3.5$), in contrast with previous reports showing an increase shortly after OI in mice CCs (Adriaenssens et al. 2011), bovine CCs (Assidi et al. 2010) and rhesus monkey whole follicles (Xu et al. 2011). This may relate to a difference

between GCs and CCs, as for example, *HAS2* has been shown to be predominant in human CCs compared to GCs (Grøndahl et al. 2012).

Follicle rupture is immediately preceded by a notable thinning of the apex with dissociation of the collagen fibrils in rabbits (Espey 1967; Dahm-Kähler et al. 2006). This restructuring has been shown to involve different proteinases, and *ADAMTS1* in particular was proven to be essential for ovulation in mice (Shozu et al. 2005; Brown et al. 2006, 2010). We found that both *ADAMTS1* and *ADAMTS9* increased strongly and peaked at 36 h. The hierarchical clustering (Fig. 5) highlights a number of highly co-regulated genes, some with an established role in follicle rupture (e.g. *SERPINE1* (Liu et al. 2004)), and some that may be worth exploring further in this context, including the protease *ECE1* and the protease inhibitor *CST3*. The small proteoglycans *DCN* and *LUM* may function in repair of the damaged tissue.

Vastly upregulated genes during ovulation with no receptors expressed in GCs might serve an extra-follicular role, for example *NTS*.

NTS is a neuropeptide, which has recently been shown to increase body temperature by an effect in the hypothalamus (Naganuma et al. 2019), and it has been suggested as a regulator of GnRH secretion (Dungan Lemko et al. 2010). Furthermore, NTS increases sperm capacitation in mice and cattle (Hiradate et al. 2014; Umezu et al. 2016) and may therefore also play a role by accompanying the oocyte into the salpinx to aid fertilization. However, whether NTS reaches the blood stream or the salpinx during ovulation in humans remain to be determined.

In the majority of women included in the present study, ovulation was induced with GnRHa (51 from 83 samples used in the microarray), and the results should therefore illustrate the ovulatory response of a combined action of both LH and FSH, similar to what occurs naturally. Furthermore, the central role of both FSH and LH as predicted by IPA in the present study, suggests that LH alone (the golden standard hCG trigger) may be short of an FSH effect, which could be important for oocyte competence or CL function. However, in the present study, treatment differences were negligible (contribution to sample variation below 3%), probably because the study was not powered to see these differences. It has been shown before at oocyte retrieval that different treatment and trigger protocols impact on GC gene expression (Grøndahl et al. 2009; Brannian et al. 2010; Borgbo et al. 2013; Gatta et al. 2013; Haas et al. 2014). However, in the present study, the time point differences by far exceeded that of the treatment differences, and only at 36 h the number of samples included ($n = 44$) provided the power to show some differences between the protocols. As shown in the present study, many genes crucial to ovulation peak early/mid-ovulation, and future studies should therefore be powered to look for differences at this time in order to reveal potential functional differences between the ovulation triggers.

We found a high overlap between DEGs in the present study and our previous study (Wissing et al. 2014) (DEGs at 0–36 h showed 80% similarity, Supplementary Table S1j). The previous cohort underwent an agonist downregulation protocol, the GCs were treated slightly differently and the microarray platform and normalization approach were different. The high overlap therefore appears to confirm the biological relevance of the findings. However, the results in both studies were obtained in a stimulated cycle and may therefore be different from a natural cycle. Well-established ovulatory factors discovered in both natural and stimulated animal experiments were vastly regulated in the present study, and overall, our results are in accordance with previous human studies in a natural cycle regarding MMP expression, PG, PGR and EGF system expression (McCord et al. 2012; Al-Alem et al. 2015; Rosewell et al. 2015; Choi et al. 2017b, 2018): this suggests that our findings may also extrapolate to events of a natural cycle.

The events of ovulation as described by transcription need confirmation on a functional level. The present dataset offers the opportunity to explore any specific process that may affect human ovulation and generate hypotheses for additional studies. Furthermore, assessment of different splice variants and differential expression of noncoding transcripts, which may play regulatory roles, were beyond the scope of this report but are available for investigation in the dataset. The major changes occurring between 0 and 12 h as observed in the present dataset invite further exploration of the early response events in order to clarify the mechanisms of OI in humans. Future studies should be aimed at dissecting this period more closely.

Conclusion

For the first time, the temporal transcriptomic changes in human GCs during ovulation were described across five different time points. The expression pattern demonstrated a two-stage process with major transcriptional upregulation peaking at 12 h and at 36 h after OI, which were dominated by genes and pathways known from the inflammatory system. Functional analyses predicted a number of upstream regulators, including both LH and FSH, which underline a potentially important role for FSH in OI. Investigation of specific systems related to tissue remodelling and oocyte maturation disclosed the timed regulation of known factors contributing to these processes, while co-regulation suggests new factors that may be of importance to human ovulation. Suggested upstream regulators and highly DEGs may be potential pharmaceutical targets in fertility treatment and gynaecology. This publicly available dataset will be valuable for future investigations of human ovarian function.

Supplementary data

Supplementary data are available at *Human Reproduction* online.

Acknowledgements

The authors thank Rehannah Borup, PhD, the Molecular Aging Program, University of Copenhagen, Denmark, for advice on the microarray and bioinformatics analyses.

Authors' roles

L.C.P. designed and executed the cohort study, included patients, isolated GCs, performed bioinformatics analyses on the raw microarray data, interpreted results and drafted the manuscript. A.L.E.G. and K.B.P. included patients and performed or supervised follicle punctures. A.L.E.G., M.L.G. and C.Y.A. conceived the idea, designed the cohort study and interpreted the results. O.Ø. performed and supervised the RNA isolation and microarray analysis and assisted with bioinformatic analyses. J.A.B. performed qRT-PCR analyses. All authors critically revised the manuscript and approved the final version.

Funding

Interreg V ÔKS through ReproUnion (www.reprounion.eu); Region Zealand Research Foundation. The funders had no role in study design, collection of data, analyses, writing of the manuscript or the decision to submit it for publication.

Conflict of interest

The authors have no conflicts of interest to disclose.

References

- Adriaenssens T, Segers I, Wathlet S, Smits J. The cumulus cell gene expression profile of oocytes with different nuclear maturity and potential for blastocyst formation. *J Assist Reprod Genet* 2011; **28**:31–40.

- Affymetrix. *Microarray Normalization Using Signal Space Transformation With Probe Guanine Cytosine Count Correction* [Internet]. 2019; Accessed date is on January 1, 2020. https://tools.thermofisher.com/content/sfs/brochures/sst_gccn_whitepaper.pdf.
- Al-Alem L, Puttabyatappa M, Rosewell K, Brännström M, Akin J, Boldt J, Muse K, Curry TE. Chemokine ligand 20: a signal for leukocyte recruitment during human ovulation? *Endocrinology* 2015; **156**:3358–3369.
- Amsterdam A. Novel genes regulated by gonadotropins in granulosa cells: new perspectives on their physiological functions. *Mol Cell Endocrinol* 2003; **202**:133–137.
- Ascoli M, Fanelli F, Segaloff DL. The lutropin/choriogonadotropin receptor, a 2002 perspective. *Endocr Rev* 2002; **23**:141–174.
- Assidi M, Dieleman SJ, Sirard M-A. Cumulus cell gene expression following the LH surge in bovine preovulatory follicles: potential early markers of oocyte competence. *Reproduction* 2010; **140**:835–852.
- Baranova NS, Inforzato A, Briggs DC, Tilakaratna V, Enghild JJ, Thakar D, Milner CM, Day AJ, Richter RP. Incorporation of pentraxin 3 into hyaluronan matrices is tightly regulated and promotes matrix cross-linking. *J Biol Chem* 2014; **289**:30481–30498.
- Barros RG, Lima PF, Soares ACS, Sanches L, Price CA, Buratini J. Fibroblast growth factor 2 regulates cumulus differentiation under the control of the oocyte. *J Assist Reprod Genet* 2019; **36**:905–913.
- Bishop CV, Hennebold JD, Kahl CA, Stouffer RL. Knockdown of progesterone receptor (PGR) in macaque granulosa cells disrupts ovulation and progesterone production. *Biol Reprod* 2016; **94**:109.
- Bolstad BM, Irizarry R, Astrand M, Speed TP. A comparison of normalization methods for high density oligonucleotide array data based on variance and bias. *Bioinformatics* 2003; **19**:185–193.
- Bomsel-Helmreich O, Huyen LV, Durand-Gasselin I, Salat-Baroux J, Antoine JM. Timing of nuclear maturation and cumulus dissociation in human oocytes stimulated with clomiphene citrate, human menopausal gonadotropin, and human chorionic gonadotropin. *Fertil Steril* 1987; **48**:586–595.
- Borgbo T, Povlsen BB, Andersen CY, Borup R, Humaidan P, Grøndahl ML. Comparison of gene expression profiles in granulosa and cumulus cells after ovulation induction with either human chorionic gonadotropin or a gonadotropin-releasing hormone agonist trigger. *Fertil Steril* 2013; **100**:994–1001.e2.
- Brannian J, Eyster K, Mueller BA, Bietz MG, Hansen K. Differential gene expression in human granulosa cells from recombinant FSH versus human menopausal gonadotropin ovarian stimulation protocols. *Reprod Biol Endocrinol* 2010; **8**:25.
- Brown GR, Hem V, Katz KS, Ovetsky M, Wallin C, Ermolaeva O, Tolstoy I, Tatusova T, Pruitt KD, Maglott DR et al. Gene: a gene-centered information resource at NCBI. *Nucleic Acids Res* 2015; **43**:D36–D42.
- Brown HM, Dunning KR, Robker RL, Boerboom D, Pritchard M, Lane M, Russell DL. ADAMTS1 cleavage of versican mediates essential structural remodeling of the ovarian follicle and cumulus-oocyte matrix during ovulation in mice. *Biol Reprod* 2010; **83**:549–557.
- Brown HM, Dunning KR, Robker RL, Pritchard M, Russell DL. Requirement for ADAMTS-1 in extracellular matrix remodeling during ovarian folliculogenesis and lymphangiogenesis. *Dev Biol* 2006; **300**:699–709.
- Carletti MZ, Christenson LK. Rapid effects of luteinizing hormone on gene expression in the mural granulosa cells of mouse periovulatory follicles. *Reproduction* 2009; **137**:843–855.
- Choi Y, Park JY, Wilson K, Rosewell KL, Brännström M, Akin JW, Curry TE, Jo M. The expression of CXCR4 is induced by the luteinizing hormone surge and mediated by progesterone receptors in human preovulatory granulosa cells. *Biol Reprod* 2017a; **96**:1256–1266.
- Choi Y, Rosewell KL, Brännström M, Akin JW, Curry TE, Jo M. FOS, a critical downstream mediator of PGR and EGF signaling necessary for ovulatory prostaglandins in the human ovary. *J Clin Endocrinol Metab* 2018; **103**:4241–4252.
- Choi Y, Wilson K, Hannon PR, Rosewell KL, Brännström M, Akin JW, Curry TE, Jo M. Coordinated regulation among progesterone, prostaglandins, and EGF-like factors in human ovulatory follicles. *J Clin Endocrinol Metab* 2017b; **102**:1971–1982.
- Christenson LK, Gunewardena S, Hong X, Spitschak M, Baufeld A, Vanselow J. Research resource: preovulatory LH surge effects on follicular theca and granulosa transcriptomes. *Mol Endocrinol* 2013; **27**:1153–1171.
- Coticchio G, Dal Canto M, Mignini Renzini M, Guglielmo MC, Brambillasca F, Turchi D, Novara PV, Fadini R. Oocyte maturation: gamete-somatic cells interactions, meiotic resumption, cytoskeletal dynamics and cytoplasmic reorganization. *Hum Reprod Update* 2015; **21**:427–454.
- Dahm-Kähler P, Löfman C, Fujii R, Axelsson M, Janson PO, Brännström M. An intravital microscopy method permitting continuous long-term observations of ovulation *in vivo* in the rabbit. *Hum Reprod* 2006; **21**:624–631.
- Donadeu FX, Fahiminiya S, Esteves CL, Nadaf J, Miedzinska K, McNeilly AS, Waddington D, Gérard N. Transcriptome profiling of granulosa and theca cells during dominant follicle development in the horse. *Biol Reprod* 2014; **91**:111.
- Duffy DM, Ko C, Jo M, Brannstrom M, Curry TE. Ovulation: parallels with inflammatory processes. *Endocr Rev* 2019; **40**:369–416.
- Dungan Lemko HM, Naderi R, Adjan V, Jennes LH, Navarro VM, Clifton DK, Steiner RA. Interactions between neurotensin and GnRH neurons in the positive feedback control of GnRH/LH secretion in the mouse. *Am J Physiol Endocrinol Metab* 2010; **298**:E80–E88.
- Espey LL. Ultrastructure of the apex of the rabbit graafian follicle during the ovulatory process I. *Endocrinology* 1967; **81**:267–276.
- Espey LL. Ovulation as an inflammatory reaction—a hypothesis. *Biol Reprod* 1980; **22**:73–106.
- Fang L, Cheng J-C, Chang H-M, Sun Y-P, Leung PCK. EGF-like growth factors induce COX-2-derived PGE2 production through ERK1/2 in human granulosa cells. *J Clin Endocrinol Metab* 2013; **98**:4932–4941.
- Gatta V, Tatone C, Ciriminna R, Vento M, Franchi S, d'Aurora M, Sperduti S, Cela V, Borzi P, Palermo R et al. Gene expression profiles of cumulus cells obtained from women treated with recombinant human luteinizing hormone + recombinant human follicle-stimulating hormone or highly purified human menopausal gonadotropin versus recombinant human follicle-stimulating hormone alone. *Fertil Steril* 2013; **99**:2000–2008.e1.
- Gilbert I, Robert C, Dieleman S, Blondin P, Sirard M-A. Transcriptional effect of the LH surge in bovine granulosa cells during the periovulation period. *Reproduction* 2011; **141**:193–205.

- Gloaguen P, Crépieux P, Heitzler D, Poupon A, Reiter E. Mapping the follicle-stimulating hormone-induced signaling networks. *Front Endocrinol (Lausanne)* 2011;**2**:45.
- Grøndahl ML, Andersen CY, Bogstad J, Borgbo T, Hartvig Boujida V, Borup R. Specific genes are selectively expressed between cumulus and granulosa cells from individual human pre-ovulatory follicles. *Mol Hum Reprod* 2012;**18**:572–584.
- Grøndahl ML, Borup R, Lee YB, Myrhøj V, Meinertz H, Sørensen S. Differences in gene expression of granulosa cells from women undergoing controlled ovarian hyperstimulation with either recombinant follicle-stimulating hormone or highly purified human menopausal gonadotropin. *Fertil Steril* 2009;**91**:1820–1830.
- Haas J, Ophir L, Barzilay E, Yerushalmi GM, Yung Y, Kedem A, Maman E, Hourvitz A. GnRH agonist vs. hCG for triggering of ovulation—differential effects on gene expression in human granulosa cells. *PLoS One* 2014;**9**: e90359.
- Hernandez-Gonzalez I, Gonzalez-Robayna I, Shimada M, Wayne CM, Ochsner SA, White L, Richards JS. Gene expression profiles of cumulus cell oocyte complexes during ovulation reveal cumulus cells express neuronal and immune-related genes: does this expand their role in the ovulation process? *Mol Endocrinol* 2006;**20**:1300–1321.
- Hiradate Y, Inoue H, Kobayashi N, Shirakata Y, Suzuki Y, Gotoh A, Roh S, Uchida T, Katoh K, Yoshida M et al. Neurotensin enhances sperm capacitation and acrosome reaction in mice. *Biol Reprod* 2014;**91**:53.
- Kim J, Bagchi IC, Bagchi MK. Control of ovulation in mice by progesterone receptor-regulated gene networks. *Mol Hum Reprod* 2009;**15**:821–828.
- Knight PG, Glister C. TGF- β superfamily members and ovarian follicle development. *Reproduction* 2006;**132**:191–206.
- Krämer A, Green J, Pollard J, Tugendreich S. Causal analysis approaches in ingenuity pathway analysis. *Bioinformatics* 2014;**30**:523–530.
- Kristensen SG, Andersen K, Clement CA, Franks S, Hardy K, Andersen CY. Expression of TGF-beta superfamily growth factors, their receptors, the associated SMADs and antagonists in five isolated size-matched populations of pre-antral follicles from normal human ovaries. *Mol Hum Reprod* 2014;**20**:293–308.
- Liu W, Xin Q, Wang X, Wang S, Wang H, Zhang W, Yang Y, Zhang Y, Zhang Z, Wang C et al. Estrogen receptors in granulosa cells govern meiotic resumption of pre-ovulatory oocytes in mammals. *Cell Death Dis* 2017;**8**: e2662.
- Liu Y-X, Liu K, Feng Q, Hu Z-Y, Liu H-Z, Fu G-Q, Li Y-C, Zou R-J, Ny T. Tissue-type plasminogen activator and its inhibitor plasminogen activator inhibitor type I are coordinately expressed during ovulation in the rhesus monkey. *Endocrinology* 2004;**145**:1767–1775.
- McCord LA, Li F, Rosewell KL, Brännström M, Curry TE. Ovarian expression and regulation of the stromelysins during the periovulatory period in the human and the rat. *Biol Reprod* 2012;**86**:78.
- Naganuma F, Kroeger D, Bandaru SS, Absi G, Madara JC, Vetrivelan R. Lateral hypothalamic neurotensin neurons promote arousal and hyperthermia. *PLoS Biol* 2019;**17**:1–27.
- Norris RP, Freudzon M, Mehlmann LM, Cowan AE, Simon AM, Paul DL, Lampe PD, Jaffe LA. Luteinizing hormone causes MAP kinase-dependent phosphorylation and closure of connexin 43 gap junctions in mouse ovarian follicles: one of two paths to meiotic resumption. *Development* 2008;**135**:3229–3238.
- Okuma A, Kuraoka A, Iida H, Inai T, Wasano K, Shibata Y. Colocalization of connexin 43 and connexin 45 but absence of connexin 40 in granulosa cell gap junctions of rat ovary. *J Reprod Fertil* 1996;**107**:255–264.
- Poulsen LC, ALM E, MLM W, Yding Andersen C, Borup R, Grøndahl ML. Human granulosa cells function as innate immune cells executing an inflammatory reaction during ovulation: a microarray analysis. *Mol Cell Endocrinol* 2019a;**486**:34–46.
- Poulsen LC, Pla I, Sanchez A, Grøndahl ML, Marko-Varga G, Yding Andersen C, ALM E, Malm J. Progressive changes in human follicular fluid composition over the course of ovulation: quantitative proteomic analyses. *Mol Cell Endocrinol* 2019b;**495**:110522.
- Rao JU, Shah KB, Puttaiah J, Rudraiah M. Gene expression profiling of preovulatory follicle in the buffalo cow: effects of increased IGF-I concentration on periovulatory events. *PLoS One* 2011;**6**: e20754.
- Richani D, Gilchrist RB. The epidermal growth factor network: role in oocyte growth, maturation and developmental competence. *Hum Reprod Update* 2018;**24**:1–14.
- Robker RL, Russell DL, Espey LL, Lydon JP, O'Malley BW, Richards JS. Progesterone-regulated genes in the ovulation process: ADAMTS-1 and cathepsin L proteases. *Proc Natl Acad Sci* 2000;**97**:4689–4694.
- Rosewell KL, Al-Alem L, Zakerkish F, McCord L, Akin JW, Chaffin CL, Brännström M, Curry TE. Induction of proteinases in the human preovulatory follicle of the menstrual cycle by human chorionic gonadotropin. *Fertil Steril* 2015;**103**:826–833.
- Shimada M, Hernandez-Gonzalez I, Gonzalez-Robayna I, Richards JS. Paracrine and autocrine regulation of epidermal growth factor-like factors in cumulus oocyte complexes and granulosa cells: key roles for prostaglandin synthase 2 and progesterone receptor. *Mol Endocrinol* 2006;**20**:1352–1365.
- Shozu M, Minami N, Yokoyama H, Inoue M, Kurihara H, Matsushima K, Kuno K. ADAMTS-1 is involved in normal follicular development, ovulatory process and organization of the medullary vascular network in the ovary. *J Mol Endocrinol* 2005;**35**:343–355.
- Subramanian A, Tamayo P, Mootha VK, Mukherjee S, Ebert BL, Gillette MA, Paulovich A, Pomeroy SL, Golub TR, Lander ES et al. Gene set enrichment analysis: a knowledge-based approach for interpreting genome-wide expression profiles. *Proc Natl Acad Sci U S A* 2005;**102**:15545–15550.
- Sutovský P, Fléchon JE, Pavlok A. F-actin is involved in control of bovine cumulus expansion. *Mol Reprod Dev* 1995;**41**:521–529.
- Umezū K, Hiradate Y, Oikawa T, Ishiguro H, Numabe T, Hara K, Tanemura K. Exogenous neurotensin modulates sperm function in Japanese black cattle. *J Reprod Dev* 2016;**62**:409–414.
- Wissing ML, Kristensen SG, Andersen CY, Mikkelsen AL, Høst T, Borup R, Grøndahl ML. Identification of new ovulation-related genes in humans by comparing the transcriptome of granulosa cells before and after ovulation triggering in the same controlled ovarian stimulation cycle. *Hum Reprod* 2014;**29**:997–1010.
- Xu F, Stouffer RL, Müller J, Hennebold JD, Wright JW, Bahar A, Leder G, Peters M, Thorne M, Sims M et al. Dynamics of the transcriptome in the primate ovulatory follicle. *Mol Hum Reprod* 2011;**17**:152–165.
- Zaiss DMW, Gause WC, Osborne LC, Artis D. Emerging functions of amphiregulin in orchestrating immunity, inflammation, and tissue repair. *Immunity* 2015;**42**:216–226.
- Zhang M, Su Y-Q, Sugiura K, Wigglesworth K, Xia G, Eppig JJ. Estradiol promotes and maintains cumulus cell expression of natriuretic peptide receptor 2 (NPR2) and meiotic arrest in mouse oocytes *in vitro*. *Endocrinology* 2011;**152**:4377–4385.